

UNCLASSIFIED

Defense Technical Information Center
Compilation Part Notice

ADP013689

TITLE: On the Application of Hybrid RANS-LES and Proper Orthogonal
Decomposition Techniques to Control of Cavity Flows

DISTRIBUTION: Approved for public release, distribution unlimited

This paper is part of the following report:

TITLE: DNS/LES Progress and Challenges. Proceedings of the Third
AFOSR International Conference on DNS/LES

To order the complete compilation report, use: ADA412801

The component part is provided here to allow users access to individually authored sections
of proceedings, annals, symposia, etc. However, the component should be considered within
the context of the overall compilation report and not as a stand-alone technical report.

The following component part numbers comprise the compilation report:

ADP013620 thru ADP013707

UNCLASSIFIED

ON THE APPLICATION OF HYBRID RANS-LES AND PROPER ORTHOGONAL DECOMPOSITION TECHNIQUES TO CONTROL OF CAVITY FLOWS

SRINIVASAN ARUNAJATESAN AND NEERAJ SINHA
Combustion Research and Flow Technology, Inc.
(CRAFT Tech) Dublin, PA 18917

LAWRENCE UKEILEY
National Center for Physical Acoustics (NCPA)
University of Mississippi
Oxford, MS

Abstract

Issues pertaining to the application of hybrid RANS-LES modeling and Proper Orthogonal Decomposition (POD) techniques to the development of control strategies for cavity flows are discussed. The criteria for correct and consistent hybrid RANS-LES modeling are outlined – unsteady RANS-LES interfacing and mesh sensitive eddy-viscosity modeling are identified as the main issues. Preliminary calculations of a compression ramp are presented to illustrate our approach for RANS-LES interfacing. Next, a generalized mesh dependent eddy-viscosity modeling procedure is detailed and its applicability is demonstrated through calculations of weapons bay cavity flows. Comparisons with measurements are seen to agree better than earlier “LES” calculations which did not adequately treat the approach boundary layer. The technique is then used to create datasets for developing a POD based model of the cavity flow field. The differences between coupled and uncoupled POD applications to the density and velocity fields are discussed – it is seen that the coupled approach yields a flow field representation that is closer to the parent LES flow field than the uncoupled approach. Finally, a dynamical systems model of the flow field is presented. Applications to control problems are now in progress and will be presented in the future.

1. Introduction

The use of passive controllers to control the aeroacoustics in weapons bay flow fields has been studied in the past with limited success and range of operability, forcing aircraft to reduce speed to deploy stores [1,2]. Active control technology presents a better alternative because of its ability to adapt to the different flow conditions and its potentially larger range of operability. Techniques such as pulsed jets, piezzo activated actuation, and more recently, high

frequency actuation as a control means have been studied [3]. While the search for an optimal controller continues, analysis techniques are sought that can be used to examine the flow field and test out the controller concepts. Towards this end, a joint research effort has been initiated at CRAFT Tech and NCPA to develop a high fidelity lower dimensional model of the weapons bay flowfield combining hybrid RANS-LES modeling and the Proper Orthogonal Decomposition (POD) technique. While modeling based on Large Eddy Simulation (LES) embodies sufficient fidelity to represent the dynamic aeroacoustic environment in a cavity [4], it requires substantive computer resources and consequently, a hybrid RANS-LES method has been developed to minimize cost and maximize computational fidelity. Lumley's Proper Orthogonal Decomposition (POD) methodology [5] is being assessed with the objective of developing a simplified model of cavity flow dynamics. This entails utilization of the numerical simulation data to obtain a simplified eigenfunction representation of the flow that is ideally suited for utilization in a Low Dimensional Model of the cavity to study control alternatives.

In this paper, two aspects of this development effort are presented. In the first part of the paper, we discuss issues pertaining to hybrid RANS-LES modeling for complex flows in general and demonstrate its application to a weapons bay flow field. The issues of interfacing between RANS and LES – an issue not addressed so far in the literature – and mesh sensitive unified turbulence modeling are discussed. In the second part of the paper, we address the development of a reduced order POD based model of the cavity flowfield based on hybrid RANS-LES simulations. Issues pertaining to the coupling of flow field variables are addressed and a general method to develop a lower dimensional dynamical model for the cavity flow field is presented.

2. Hybrid RANS-LES Modeling

In the first of the present series of conferences, Spalart et al. [6] estimated (optimistically) that an LES of a whole aircraft flow field would require about 10^{11} grid points and about 5 million time steps to obtain reasonable solutions. Simulations using just a fraction of that number of grid points are still not possible today. Hybrid RANS-LES methods address this need by combining the cost effectiveness of RANS methods with the accuracy of LES methods. RANS methods compute only the mean flow field while modeling the effects of turbulence entirely. LES methods, on the other hand, resolve most of the energy containing flow scales and model only the small turbulent scales. RANS methods are thus suitable only for steady or at most mildly unsteady flows, while, LES methods perform much better for flowfields with strong unsteadiness. Hybrid RANS-LES methods attempt to take advantage of this fact by resorting to RANS type modeling in steady flow regions and switching to LES type modeling only in regions where it is required (such as regions with strong unsteadiness, separation

or aeroacoustic interactions, etc). However, interfacing RANS and LES regions of the flow fields is not straightforward and requires careful examination.

In order to interface RANS and LES solutions consistently, two different aspects need to be considered. The first one pertains to the fact that the RANS solutions are steady solutions while the LES solutions are unsteady. Hence, when RANS solutions are used as interfacial boundary conditions (either implicitly through unified methods or explicitly by zonal methods) the steady state flow field needs to be augmented with unsteady fluctuations. This has to be done in a manner consistent with the LES resolution at the interface boundary. Secondly, the eddy viscosity that is used to model the effects of the unresolved scales (all turbulent scales in RANS and sub-grid scales in LES) has to be suitably modified to reflect the increased resolution in LES regions. Unless both these conditions are satisfied, truly hybrid RANS-LES interfacing cannot be achieved. In the literature to date, several hybrid approaches [6,7,8,9,10] have been proposed to address the second issue, while the first issue has not received much attention. In all these methods, the eddy viscosity computation is suitably tuned such that a certain extent of mesh dependence is achieved – regions of higher resolution (or LES type regions) see lower values of the turbulent viscosity while regions of lower resolution (or RANS type regions) see higher turbulent viscosities. Thus steady solutions are obtained in regions of lower resolution while a higher level of unsteadiness is sustained in regions of higher resolution.

While this approach is consistent with the general dissipative natures of RANS and LES, it does not reconcile the large differences in the range of structures resolved in the RANS and LES regions. This omission can be unimportant to a large class of problems where the unsteadiness is generated and contained entirely within the LES domain (such as cavity flows, as we will show later), but can be very important for a wide class of problems where the small scales unsteadiness that are not resolved in the RANS regions interact very strongly with the flow structures in the LES regions. In the RANS region, only the mean flow field is resolved and all turbulence is modeled – the structure of the turbulent flow field is represented by increased turbulent diffusivities and kinetic energy, thus capturing the turbulence effect in a statistical sense. However, such a representation does not allow for the unsteady interactions of any flow structures in the RANS regions with any other flow field characteristics in the LES region. Hence, the resulting solution in the LES region cannot capture any of the unsteadiness present in the actual flow field. For such flows, the mean flow field from the RANS solution must be transformed at the interface boundary to re-introduce the unsteadiness in the flow field, so that the LES region will see the proper boundary conditions.

In the next section, we present two example calculations – one of each of the types discussed above. The first calculation is that of a supersonic flow over a

compression corner – this is shown to demonstrate the importance of the unsteadiness re-creation concept discussed earlier. The second flow field, discussed in more detail, is the hybrid simulation of the cavity flow field. In this flow, the effect of the small scale unsteadiness in the upstream boundary layer is small – the flow is dominated by resonant shear layer-acoustic interactions in the cavity. For this flow field, the mesh dependent eddy viscosity modeling methodology is demonstrated.

2.1 Unsteady Interfacing for Hybrid RANS-LES

In this section we present an example of a flowfield where the interaction of the unsteadiness in the “RANS” region of a hybrid simulation strongly affects the “LES” region simulation. This calculation is presented here only as a demonstration of the issue of

interfacing – the details are omitted for brevity and will be presented elsewhere. The flow field chosen for this purpose is a Mach 2.88 flow over a compression corner (Fig. 1) – a flat plate boundary layer (with a long run) leads up to a ramp with a turning angle of 8 degrees. Here, results from two calculations are shown - in both these calculations, the upstream approach boundary layer is simulated using RANS (using a $k-\epsilon$ turbulence model) and a short distance upstream of the compression corner the model is switched to LES (a one equation LES model [10] is used). In the first simulation, nothing is done at the interface between the RANS and LES regions, the RANS profile is used as the starting input profile for the LES calculation. In the second simulation, the RANS boundary layer is transformed into an LES boundary layer using the recycling method of Urbin and Knight [11]. The mean boundary layer thickness at the interface location for the two calculations is the same; the only difference is the unsteadiness in the flow field in the second simulation.

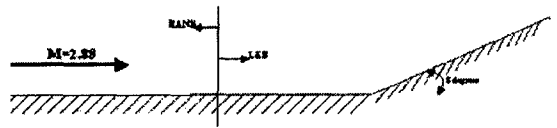


Fig. 1. Schematic of the compression ramp calculation

interfacing – the details are omitted for brevity and will be presented elsewhere. The flow field chosen for this purpose is a Mach 2.88 flow over a compression corner (Fig. 1) – a flat plate boundary layer (with a long run) leads up to a ramp with a turning angle of 8 degrees. Here, results from two calculations are shown - in both these calculations, the upstream approach boundary layer is simulated using RANS (using a $k-\epsilon$ turbulence model) and a short distance upstream of the compression corner the model is switched to LES (a one equation LES model [10] is used). In the first simulation, nothing is done at the interface between the RANS and LES regions, the RANS profile is used as the starting input profile for the LES calculation. In the second simulation, the RANS boundary layer is transformed into an LES boundary layer using the recycling method of Urbin and Knight [11]. The mean boundary layer thickness at the interface location for the two calculations is the same; the only difference is the unsteadiness in the flow field in the second simulation.

Figures 2 and 3 show an instantaneous snapshot of the shock structure in the corner – the effect of the unsteadiness is clearly seen in Fig. 3 – the streamwise vortices in the boundary layer wrinkle the shock surface and cause the shock to



Fig. 2. Instantaneous snap shot from the hybrid calculation without unsteady interfacing.



Fig. 3. Instantaneous snap shot of density contours from the hybrid calculation with unsteady interfacing following ref. [11].

constantly move about its mean location. Figure 2 on the other hand does not show any unsteadiness at all – the shock is stationary, and no fluctuations are visible in the flow field. Further, the recirculation length is incorrect and in fact, moves all the way upstream to the inflow boundary before the simulation has to be stopped. The comparison of the surface pressures shows that the second simulation yields much better comparisons with the experimental data and the LES of Yan et al. [12]. This shows that the small structures in the upstream boundary layer can be very important in predicting this flow field. These small scale structures provide the turbulent mixing (diffusion) that keeps the shock stably oscillating around its mean position. In the case of the pure LES, this turbulent diffusion is missing and the shock moves all the way upstream. Therefore, the unsteadiness not only is responsible for providing the shock (and hence the pressure oscillations), it is also responsible for the stability of the flowfield itself.

2.2 Mesh Dependent Turbulence Modeling for Hybrid RANS-LES

In this section we describe a method for introducing a mesh dependence in the computation of the eddy viscosity used in turbulence models. The model is based on the k - ϵ RANS model and the one-equation subgrid model [10]. As we shall show, the model reduces to the baseline RANS model in regions where the mesh does not permit the resolution of flow structures. As the mesh size decreases in regions of strong flow features, the model reduces to the LES model thereby allowing the user to perform hybrid calculations within a unified framework. Clearly, this is more suited to problems that are not strongly dependent upon the interfacing boundary conditions. To demonstrate the applicability of this model, we apply it to the simulation of a weapons bay flow field – these results are presented in the next section.

As mentioned earlier, several approaches have been proposed to deal with mesh dependent eddy viscosities [6-10]. However, as identified in Reference [8], one drawback of the approaches is that no attempt is made to determine the extent of the local resolution with respect to the overall turbulence levels. A certain grid size will resolve different amounts of energy/turbulence in low and high Reynolds number flows. That this relative difference in the resolution with respect to the local turbulence levels is incorporated into the various hybrid models is not clear. In order to address this issue, we present a different approach here. In this method, the eddy viscosity is still linked to the local mesh size; however, additional effort is spent to characterize the local turbulence levels, so that the amount of net turbulent dissipation used in the momentum and energy balance is consistent with the local mesh size *and* the local turbulent Reynolds number.

The overall approach involves solving the mass, momentum and energy conservation equations using a finite volume framework. In addition to these conservation equations, two additional equations describing the evolution of the

turbulence variables are solved for - one each for the subgrid kinetic energy and the overall turbulent dissipation rate, respectively. These equations are given as follows:

$$\begin{aligned} \frac{\partial \rho k^{sgs}}{\partial t} + \frac{\partial}{\partial x_i} \left(\rho \mu_i k^{sgs} - \left(\mu + \frac{\mu_T^{SGS}}{\sigma_k} \right) \frac{\partial k^{sgs}}{\partial x_i} \right) &= P_k - \rho \epsilon^{sgs} \\ \frac{\partial \rho \epsilon}{\partial t} + \frac{\partial}{\partial x_i} \left(\rho \mu_i \epsilon - \left(\mu + \frac{\mu_T^{RANS}}{\sigma_\epsilon} \right) \frac{\partial \epsilon}{\partial x_i} \right) &= P_\epsilon - D_\epsilon \end{aligned} \quad (1)$$

Here, σ_k , σ_ϵ , are the modeling constants appearing in the RANS form of the k - ϵ model. Details of the expressions for the source terms on the right hand side of equation (1) are presented in Ref. [8] and are omitted here for brevity. Note that since the two quantities represent different scale variables, namely, ϵ represents the large scale variable and k^{sgs} represents the sub-grid scales (SGS), different eddy viscosities are used in the two equations. The momentum and energy equations, however, use the SGS value of the eddy viscosity because that represents the amount of energy that is dissipated from the flow field based on how much of the flow field is resolved. This value blends to the RANS value as the grid is coarsened, as will be shown later.

Once these two variables are available at any flow field location, it is assumed that the local turbulent energy spectrum can be represented using a hybrid form of the energy-inertial-dissipation range spectrum. The form of the spectrum is given as follows,

$$\hat{E}(\hat{k}) = C_e \hat{k}_e^{-5/3} \left(\frac{\hat{k}}{\hat{k}_e} \right)^4 \left(1 + \left(\frac{\hat{k}}{\hat{k}_e} \right)^2 \right)^{-17/6} \exp\left(-\frac{3}{2} \alpha \hat{k}^{4/3}\right) \quad (2)$$

where, $\alpha=1.5$, $\hat{k} = k\eta$, and $\hat{E} = E / (v^5 \epsilon)^{1/4}$. Here, k is the wave number, \hat{k}_e is an energy containing wave number, and C_e is a constant to be determined. The calibration for C_e requires that the integral of the dissipation range spectrum yield the local turbulence dissipation rate. In order for this form to be useful, the independent variables, namely, η the Kolmogorov scale and \hat{k}_e , in equation (2) must be related to the flow variables. The Kolmogorov scale is computed from the turbulent dissipation rate and laminar viscosity

Information about the subgrid kinetic energy and the Δ , the local mesh resolution are used to compute the energy containing wave number \hat{k}_e .

$$k^{SGS} = \int_{k_\Delta}^{\infty} E(k) dk \quad (3)$$

Equation (2) can be solved iteratively to determine \hat{k}_e . This completely determines the spectrum in Equation (2) and can then be used to compute the eddy viscosities. The eddy viscosities are computed from expressions similar to the baseline RANS model expressions. The model, its testing and validations in the RANS and LES limits are described in greater detail in reference [8] and are omitted here for brevity. We now present an application of this modeling to the simulation of cavity flows. As we shall demonstrate the flow field is very amenable to this kind of modeling because the source of the unsteadiness is completely contained in the LES region. The flow field does not strongly depend on the detailed structure of the approach boundary layer, but only on the momentum thickness.

2.3 Hybrid Simulation of Cavity Flowfield

The case selected for demonstration of the hybrid LES-RANS turbulence model corresponds to an experiment performed by Shaw at the Lockheed Compressible Flow Wind Tunnel (CFWT) [13]. The tests featured a generic 20% rectangular cavity - 36 inches in length with a L/D ratio of 6. Dynamic load spectra were obtained at various locations during these tests. A schematic of the geometry and the dynamic pressure measurement locations is shown in Fig. 4. The case simulated has a freestream Mach number of 1.5 and a Reynolds number of 7 million per foot.

The weapons bay flow field can be visualized as the combination of the two flow fields discussed above - the upstream region of the cavity is a boundary layer flow field, while the flow over the cavity itself is a shear layer flow field. The goal is to achieve a RANS type behavior in the upstream boundary layer region and a LES type behavior in the shear layer region. Hence, the mesh used in the calculations are created with high aspect ratio cells in the boundary layer - the wall normal mesh spacing is fine while the axial spacing is fairly coarse. This permits the shear in the wall normal direction to be adequately resolved, but the high aspect ratio cells do not permit the resolution of the fine scale structures in the buffer region. In the shear layer over the cavity, the mesh is uniformly fine in both the directions. In this

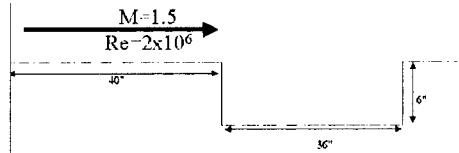


Fig. 4. Schematic of the cavity flow field.

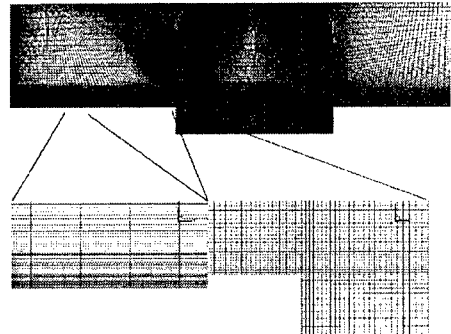


Fig. 5. Mesh used in the hybrid cavity calculation.

region, the evolution of the shear layer disturbances that result in the formation of the shear layer need to be resolved along with the strong gradients in the mean flow. The mesh used in these simulations is shown in Fig. 5. The insets show the cells in the boundary layer and shear layer regions. The wall normal resolution of $\Delta y^+ = 0.25$ was used in the boundary layer grid and the stretching rate in the boundary layer in the wall normal direction was limited to 4%. In the shear layer region over the cavity, the stretching rates in both directions were kept below 4%.

According to the test measurements, the upstream boundary layer thickness is an inch, which is consistent with one-fifth scaling for a fighter aircraft like the F-111. The dependence of the shear layer over the cavity on the boundary layer thickness has been well documented [14] – the momentum deficit at the leading edge of the cavity is critical for the shear layer development. The feedback mechanism, which determines the pressure and dynamic load fluctuations on the weapons bay floor interacts strongly with the separating boundary layer at the leading edge. Thus it is important that the boundary layer be captured accurately.

Fig. 6 shows a snapshot of the instantaneous contours of vorticity. The basic features of the flow are highlighted in this. The boundary layer upstream of the cavity is steady like a RANS boundary layer, the shear layer over the cavity, on the other hand is seen to be inherently unsteady and dominated by periodic vortex shedding from the separated boundary layer. Examination of the temporal fluctuations in the boundary layer showed that the fluctuations were barely noticeable – apart from the initial transients during start up of the calculation, there are no fluctuations in the boundary layer region upstream of the cavity leading edge. The approach boundary layer is seen to thicken with length as it approaches the cavity – the thickness of the boundary layer measured at the leading edge of the cavity (the last grid point before the cavity leading edge) shows a value of 1.067 inches. This is very close to the thickness measured in the experiments.

The shear layer over the cavity as seen from above is clearly unsteady. The separated boundary layer becomes unstable and rolls up into vortices. These vortices are convected downstream in the shear layer and impinge upon the aft end of the cavity. This causes a recirculating flow region to be set up inside the cavity forming the feedback loop. The reflected waves interact with the vortex shedding upstream, resulting in the creation of a limit cycle type process. An examination of

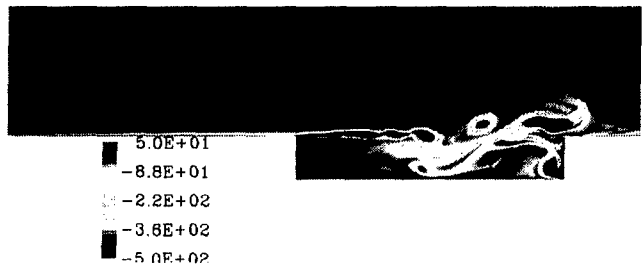


Fig. 6. Vorticity contours over the cavity showing steady RANS like and unsteady LES like regions.

the flow variables in the shear layer clearly reveals this. Of particular interest to us is the pressure oscillation in the cavity. The predicted pressure oscillations on the cavity floor are compared with experimental data.

Prior to presenting the dynamic load predictions from the present simulation, Fig. 7(a) shows predictions from a preliminary LES simulation where the entire flow field is modeled through the use of the one equation LES model [10]. The mesh used for this calculation is the same as that used for the hybrid calculation. In the pure LES calculation, the approach boundary layer is not captured correctly. There is no unsteadiness in the boundary layer because the mesh cannot sustain it, however, the thickness at the cavity leading edge and the growth rate are predicted incorrectly by this model. The boundary layer thickness at the cavity leading edge is only 0.48 inches – almost half the experimental value. This adversely effects the shear layer and the whole cavity flow field downstream of the leading edge. The predicted pressure spectra at 25% and 75% cavity length are compared with the wind tunnel data. While the overall comparison with data is reasonable, significant discrepancies can be identified.

In Fig. 7 (b) and (c), the predictions from the hybrid model are shown. The main difference between these two simulations is the boundary layer upstream of the cavity. The difference in the pressure spectra predictions is clear – the hybrid model captures both the modes and the amplitudes of the pressure oscillations very well. The pure LES calculation, on the other hand, while exhibiting the correct trends, shows significant discrepancies with the experimental measurements. This highlights the role of the boundary layer in altering the cavity feedback mechanism and is very significant for control-oriented applications of the simulation methodology.

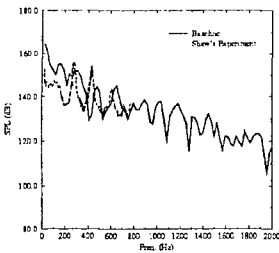


Fig. 7(a). Pressure spectrum from the pure LES at $\frac{1}{4}$ cavity length location compared with experiment.

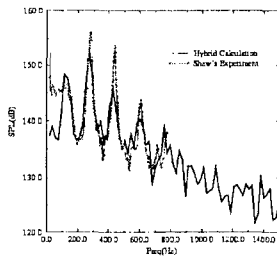


Fig. 7(b). Pressure spectrum from the hybrid RANS-LES at $\frac{1}{4}$ cavity length location compared with experiment.

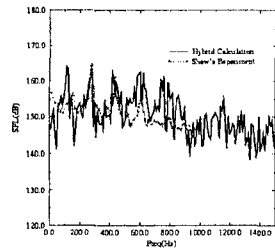


Fig. 7(c). Pressure spectrum from the hybrid RANS-LES at $\frac{3}{4}$ cavity length location compared with experiment.

In order to illustrate the role of the hybrid model, Fig. 8(a) shows contours of mean eddy viscosity and velocity in the boundary layer upstream of the cavity.

It is clearly seen that as the mesh resolution increases approaching the leading edge of the cavity the eddy viscosity drops, but there is no noticeable difference in the mean velocity contours –

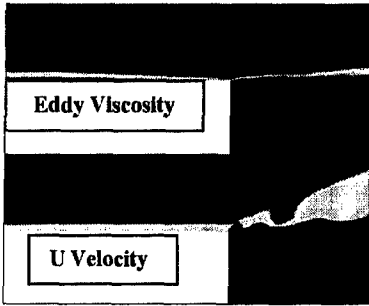


Fig. 8(a). Contours of eddy viscosity and U-velocity over the upstream

Boundary layer

through the subsonic portion of

layer there by causing oscillations in the flow variables. However, farther upstream, these are wiped out by the eddy viscosity yielding a steady boundary layer there. The time histories of the streamwise velocity at three different locations upstream of the cavity are shown in Fig. 8(b) – at the location farthest from the cavity, the oscillation amplitudes are mild and only low frequencies are seen to exist. However, as the cavity is approached, the amplitude and frequency content of the velocity fluctuations are seen to increase, this corresponds to the reduction in eddy viscosity, showing that the lower turbulent dissipation levels allows greater amounts of unsteadiness to be sustained in the boundary layer. This clearly highlights the role of the hybrid model and shows that the sought behavior has been achieved in the flow field.

So far we have discussed methods of simulating the weapons bay flow field using hybrid techniques. The goal of these simulations is to develop a greater understanding of the flow field dynamics thereby permitting us to control its behavior. However, real time control in the hybrid RANS-LES simulations is still not feasible and hence reduced order models are required to help us examine control strategy alternatives. We now present results from our approach to develop one such model using POD and the simulations described above.

3.0 Proper Orthogonal Decomposition Analysis

The low-dimensional model developed here is derived using modes from the application of the Proper Orthogonal Decomposition to the cavity data set. The basis set of the POD modes are projected onto the governing partial differential equations (PDE) using a Galerkin method. The methodology to derive

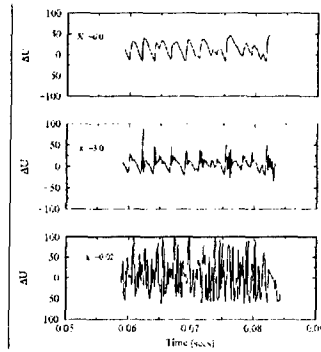


Fig. 8(b). Unsteady histories of velocity in the upstream boundary layer.

the boundary layer thickness and profile itself are not affected. Instead, an increased level of unsteadiness is seen in the boundary layer as the cavity is approached. The oscillations of the shear layer feedback

the boundary

the dynamical systems model discussed here is similar to that of Aubry et al [15] and Ukeiley et al [16]. In what follows we will briefly discuss the results of applying the POD to the numerical data-set of the cavity then discuss the formulation of the low-dimensional model. Since the cavity flow field under study is compressible the POD has been applied to both the density and velocity fields.

3.1 Application of the POD

Applications of the POD to the unsteady simulations have been reported in Ukeiley et al [16], Sinha et al [17] and Ukeiley et al [18]. All these applications follow the original work of Lumley [5], which is derived from projecting a candidate structure on the instantaneous field and maximizing in a least square sense. This results in a Fredholm integral equation, the solution of which yields the orthogonal basis vectors and the relative weights of these vectors that optimally describe the chosen field. This was later generalized to the "method of snapshots" by Sirovich [19] where he showed that the eigenfunctions of the POD can be written as linear combination of instantaneous flow fields,

$$\phi_i^n(\vec{x}) = \sum_{k=1}^M \psi^n(t_k) u_i(\vec{x}, t_k) \tag{4}$$

and they can be evaluated by solving an intermediate eigenvalue problem. This requires identifying the eigenfunctions of a matrix which is calculated by correlating independent snapshots and integrating over the spatial domain of interest. Significantly, this results in an eigenvalue problem which is of the order of the number of ensembles, and not the number of spatial locations, as with the original formulation. Equation (4) can be solved either independently for each flow variable or through the use of a suitable kernel that combines flow variables. Following Lumley and Poje [21] we have used $w = \left[\left\{ \frac{au_i}{u} \right\}_{i=1..3}, \left\{ \frac{b\rho}{r} \right\}_{i=4} \right]; u^2 = \langle u_i u_j \rangle; r^2 = \langle \rho^2 \rangle$ such that a and b satisfy $a^2 \langle u_i u_j \rangle + b^2 \langle \rho^2 \rangle = 2$ thereby modifying equation (4) as

$$\phi_i^n(\vec{x}) = \sum_{k=1}^M \psi^n(t_k) w_i(\vec{x}, t_k) \tag{5}$$

The effects of using the modified kernel as opposed to the independent decomposition will be discussed briefly here. Figure 9 shows the convergence of the POD applied to both the density and velocity fields. Approximately 20% of the mean square energy is contained in the in the dominant mode and 70% in the dominant mode and 70%

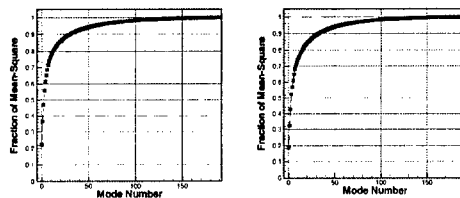


Fig. 9. Convergence of POD for density and u velocity.

in the first eight modes. The spatial structure of the modes is shown in Fig. 10(a) which shows the first 4 POD modes of streamwise velocity. The dominant modes are seen to contain information about the large scale features of the flow while the higher modes contain much of the smaller scale detail in the flow field. The vortical structure seen in the results of the hybrid calculation are seen here through an opposition in sign of eigenfunction across the shear layer. Figure 10(b) shows the modes associated with the density field. As with the velocity field, streamwise aligned waves and waves propagating out of the cavity can be distinctly identified in these modes. Shown in Fig. 11 is the effect of using the coupled formulation as opposed to the uncoupled formulation originally proposed. Here it is seen that that first modes are very different for the two reconstructions, however, as more modes are added, the solutions seem to converge. From a qualitative examination of the flowfields using only one POD mode, it is seen that the coupled application yields a reconstruction that is closer to the original flowfield, in spite of the fact that the first modes from the independent reconstructions actually contained a greater fraction of the mean square energy. Thus this implies that in order to predict the dynamics of the flow field, the coupled application yields better results.

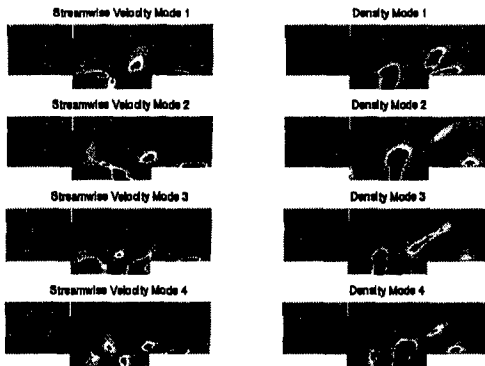


Fig. 10(a). POD modes of the velocity field from the coupled formulation.

Fig. 10(b). POD models of the density field from the coupled formulation

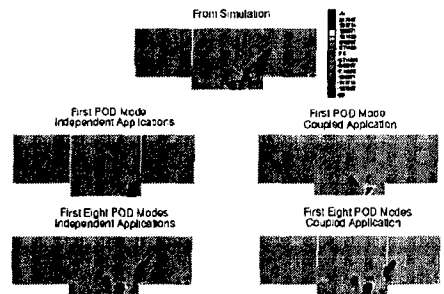


Fig. 11. Comparison of the reconstructed flow field from the coupled and uncoupled POD applications

3.2 Dynamical Systems Model

The system of PDE's for the model developed here consists of the conservation of mass and momentum equations for a compressible fluid and are given by,

$$\frac{\partial \rho}{\partial t} + \rho \frac{\partial u_j}{\partial x_j} + u_j \frac{\partial \rho}{\partial x_j} = 0 \tag{6}$$

$$\rho \frac{\partial u_i}{\partial t} + \rho u_j \frac{\partial u_i}{\partial x_j} = -\frac{\partial p}{\partial t} + \mu \frac{\partial^2 u_i}{\partial x_j \partial x_j} + \frac{1}{3} \mu \frac{\partial^2 u_j}{\partial x_i \partial x_j} \quad (7)$$

In using this system as the governing equations we are assuming a constant total enthalpy flow for the model. The first step in deriving the model equations is to expand out the density and velocity in terms of the POD modes. These representations can be written as follows,

$$\begin{aligned} u_i &= \sum_{n=1}^N a^n(t) \phi_i^n(\bar{x}) \\ \rho &= \sum_{l=1}^N b^l(t) \psi^l(\bar{x}). \end{aligned} \quad (8)$$

Since only the density and velocity will be expanded in terms of POD modes we will use an Ideal Gas assumption to relate the pressure field in terms of one of the model variables. After substituting in the above relationship the Galerkin projection is performed. The projection takes advantage of the POD basis being orthogonal to simplify the constant matrices. The resulting equations have the form,

$$\frac{\partial b^m}{\partial t} = -\sum_n a^n C1 - \sum_l b^l B1 - \sum_l \sum_n (b^l - \overline{b^l})(a^n - \overline{a^n}) B2 - \sum_l b^l B3 - \sum_l \sum_n (b^l - \overline{b^l})(a^n - \overline{a^n}) B2 \quad (9)$$

for the continuity relationship and,

$$\begin{aligned} \frac{d}{dt} a^m &= -\sum_p \sum_n b^p C3 - \sum_n a^n L1 - \sum_p \sum_n b^p a^n L2 - \sum_p \sum_n a^n a^p Q1 \\ &- \sum_p \sum_n \sum_l b^p a^n a^l Q2 + \sum_n \sum_l \overline{a^n a^l} S1 + \sum_p \sum_n \overline{b^p a^n} S2 + \sum_p \sum_n \sum_l \overline{b^p a^n a^l} S3 \end{aligned} \quad (10)$$

for the Navier-Stokes equations. In the above equations C1-C3, B1-B3, L1, L2, Q1, Q2 and S1-S3 are constant matrices calculated from the POD eigenfunctions. These coefficients relate to the various properties of the governing PDE's. For example, the linear term, L1, contains two parts; the first is viscous dissipation, the second has mean gradients which relates it to production of turbulence. It should be noted that separating the time and spatial dependence allows for the coefficients involving the POD eigenfunctions to be calculated only once since all of the time dependence is in the expansion coefficients.

3.3 Solution Methodology

Based on the results from the application of the POD the low-dimensional model developed will use 8 density and 8 velocity POD modes. This yields a set of 16 ordinary differential equations which need to be solved: 8 from continuity

and 8 from Navier-Stokes. These 16 equations have been programmed into a fourth order Runge-Kutta routine with adaptive time stepping. The routine will be used to integrate the ODE' s to obtain the expansion coefficients $a(t)$ and $b(t)$. Once the time evolution of these coefficients has been obtained they can be projected onto the eigenfunctions to get the time dependent velocity and density fields. This allows us to study both the time evolution of the dominant features and supplies a simple set of ODE' s that can be coupled with an active flow control methodology to determine an optimal flow control situation.

From examining the equations it is apparent that there are several terms that can not be written in terms of the POD modes, such as the temperature, the mean velocities and mean density. The temperature field will be assumed to be a function of space only, i.e., $T = T(\vec{x})$. This means that the temperature field will not be a function of time and in the model the mean value from all of the snapshots will be used. This is consistent with a constant total enthalpy assumption, which also allows us to only use the continuity and Navier-Stokes equations with out the energy equation. For the initial approach both the density and velocity fields will be treated as not being a function of time either. The numerical values used for these parameters will be those from the ensemble average of the snapshots. These values might be high, however, since there is over 80% of the turbulent kinetic energy and mean-square density retained in the model it is a reasonable first step. In the future a model for the mean velocity that more accurately represents an appropriate one for the truncated system and allows feedback from the turbulence can be introduced such as the one discussed in Ukeiley and Glauser, 1995.

Another important aspect of low-dimensional modeling is how to account for the neglected POD modes. To date we have tried to treat this simulation much like the VLES simulations that were used to generate the data used to extract the POD modes. That is to say, the numerical dissipation will be assumed great enough to account for energy lost to the POD modes that have not been included in the model. This is an initial approach and it is envisioned that an extra term to account for the truncated modes, much like what has been classically done, will be added later.

4.0 Conclusions and Future Work

In this paper we have addressed some key issues pertaining to the development and assessment of control strategies for cavity flows. Requirements for hybrid RANS-LES modeling in general have been outlined and demonstrative calculations have shown the need for each one of the components of hybrid modeling. The interfacial boundary condition generation issue was addressed briefly – further enhancements and improvements are being studied and will be presented in the future. The issue of mesh dependent modeling was demonstrated through its application to the cavity problem. In this regard, a more complete three

equation version of this model is being currently studied and will be presented in the future. The technique of POD was shown to be a good candidate for the application to the development of a lower dimensional model for the cavity – convergence of the POD modes was demonstrated along with comparisons to with the Hybrid RANS-LES calculations to show that the model mimics the simulations. The dynamical systems model of the flow field was derived and will be tested and studied in more detail in the future.

References

- [1] Shaw, L., Bartel, H., and McAvoy, J., "Acoustic Environment in Large Enclosures With a Small Opening Exposed to Flow," *J. of Aircraft*, Vol. 20, No 3, March 1983.
- [2] Shaw, L., "Weapons Bay Acoustic Environment Control," CEAS/AIAA -95-141, 1995.
- [3] Stanek, M.J., Raman, G., Kibens, V., Ross, J.A., Odedra, J., Peto, J.W., "Control of Cavity Resonance through Very High Frequency Forcing", AIAA -2000-1905, 2000.
- [4] Sinha, N., York, B.J., Dash, S.M., Chidambaram, N., and Findlay, D., "A Perspective on the Simulation of Cavity Aeroacoustics," AIAA Paper No. 98-0286, 1998.
- [5] Lumley, J.L., "The Structure of Inhomogeneous Turbulent Flows," *Atmospheric Turbulence and Radio Wave Propagation*, Yaglom and Tatarsky eds. Nauka, Moscow, 166-178, 1967.
- [6] Spalart, P.R., Jou, W-H., Strelets, M., and Allmaras, S.R., "Comments on the feasibility of LES for wings, and on a Hybrid RANS/LES approach", *Advances in DNS/LES, First AFOSR International conference in DNS/LES*, Greyden Press, 1997.
- [7] Speziale, C.G., "Turbulence Modeling for Time-Dependent RANS and VLES: A Review," *AIAA J.*, Vol. 36, No. 2., p 173, February 1998.
- [8] Arunajatesan, S.A. and Sinha, N., "Unified Unsteady RANS-LES Simulations of Cavity Flowfields," AIAA Paper No. 2001-0516, 39th AIAA Aerospace Sciences Meeting, Reno, NV, January 8-11, 2001.
- [9] Peltier, L.J., Zajackowski, F.J., and Wyngaard, J.C., "A Hybrid RANS/LES Approach to Large-Eddy Simulation of High-Reynolds Number Wall bounded Turbulence," FEDSM2000-11177, 2000.
- [10] Arunajatesan, S., Sinha, N., and Menon, S., "Towards Hybrid LES-RANS Computations of Cavity Flowfields", AIAA-00-0401, 38th AIAA Aerospace Sciences Meeting at Reno, NV, Jan 10-13, 2000.
- [11] Urbin, G. and D. Knight, "Compressible Large Eddy Simulation Using Unstructured Grid: Supersonic Boundary Layer", Second AFOSR International Conference on DNS and LES, Rutgers University, June 1999. Kluwer Academic Publishers, 1999, pp. 443--458. Accepted for publication in AIAA Journal.
- [12] Yan, H., Urbin, G., Knight, D., and Zheltovodov, A., "Compressible Large Eddy Simulation Using Unstructured Grid: Supersonic Boundary Layer and Compression Ramps," 10th Intl Conf. on Methods of Aerophysical Res., Institute of Theoretical and Applied Mechanics, Russ. Acad of Sciences, 2000.

- [13] Shaw, L.L., 'High Speed Application of Active Flow Control for Cavity Acoustics', AIAA-00-1926, 2000.
- [14] Dix, R.E. and Bauer, R.C., 'Experimental and Predicted Amplitudes In A Rectangular Cavity,' AIAA 2000-0472, 38th AIAA Aerospace Sciences Meeting at Reno, NV, Jan. 10-13, 2000.
- [15] Aubry, N., Holmes, P., Lumley, J. and Stone, E., 'The Dynamics of Coherent Structures in the Wall region of a Turbulent Boundary Layer', *Journal of Fluid Mechanics*, Vol. 192, 1988, 115-173.
- [16] Ukeiley, L., et al. 'Examination of Large Scale Structures in a Turbulent Plane Mixing Layer. Part 2: Dynamical Systems Model,' *J. of Fluid Mechanics*, Vol. 441, pp. 67-108, 2001.
- [17] Sinha, N, and Arunajatesan, S., and Ukeiley, L., 'High Fidelity Simulation Of Weapons Bay Aeroacoustics Attenuation Using Active Flow Control,' Paper No. AIAA-2000-1968, 6th AIAA/CEAS Aeroacoustics Conference, Lahaina, Hawaii, June 12-14, 2000.
- [18] Ukeiley, L., Kannepalli, C., Arunajatesan, S. and Sinha, N. 'Low-Dimensional Description of Variable Density Flows'. AIAA Paper 2001-0515, 39th AIAA Aerospace Sciences Mtg, Reno, NV, Jan., 2001.
- [19] Sirovich, L., 'Turbulence and the Dynamics of Coherent Structures,' *Quarterly of Applied Math*, 45 (3), 1987.
- [20] Lumley, J.L. and Poje, A.J., 'Low-Dimensional Models for Flows with Density Fluctuations', *Physics of Fluids*, Vol. 9, No. 7, 2023-2031, 1997.